Frequency-Correlation Analysis of PMD Emulators With Symmetric Polarization Scrambling

Leigh Palmer, *Student Member, IEEE*, Peter M. Farrell, Sarah D. Dods, *Senior Member, IEEE*, and Jamie S. Evans, *Member, IEEE*

***Abstract*—The authors investigate the artificial frequency correlation induced by polarization scrambled statistical polarization-mode-dispersion emulators. A simple model is derived that accurately predicts the average frequency correlation when the scrambling is symmetric. It is shown that the nature of the symmetry affects the emulator performance, and that increasingly, isotropic scrambling gives lower correlation. The derived model shows a good agreement with Monte Carlo simulation and experiment.**

***Index Terms*—Autocorrelation function (ACF), emulation, optical communication, polarization mode dispersion (PMD).**

I. Introduction

POLARIZATION mode dispersion (PMD) is a key source of signal degradation impeding the upgrade of optical links to transmission rates of > 10 Gb/s. While fiber with ultralow PMD (≤ 0.04 ps/$\sqrt{\text{km}}$) is commercially available for laying new long-haul high-speed links, previously installed legacy fibers may have much larger PMD coefficients and require active PMD compensation [1]. Therefore, characterizing the effects of PMD in a system, as well as testing PMD-mitigation strategies, remains an active area of research.

Statistical PMD emulators [2] play an important role in PMD analysis. Along with deterministic-PMD sources [3], they allow systematic PMD to be efficiently inserted in a link testbed. Ideally, emulators should accurately reproduce the statistics of the PMD that a signal would see on a real link, as well as have good stability and repeatability. However, one consideration often overlooked is how well they reproduce the joint-PMD statistics across an entire spectrum of wavelength-division-multiplexing (WDM) channels. Currently, most statistical emulators are constructed by concatenating a relatively small number of strongly birefringent elements and randomly varying the mode coupling between them to generate an ensemble of different PMD states, typically by tuning the birefringent phase of the elements [4] or rotating the polarization state between them [2], [5], [6] (see Fig. 1). A drawback of this design is that the PMD emulated for different channels tends to be correlated due to the discrete structure of the device. Artificial frequency correlation between channels affects the joint-channel-outage probabilities [7], while correlation within the bandwidth of a single channel can also affect the higher order PMD statistics [2]. Combined, these two effects compromise the use of these PMD emulators for WDM system analysis.

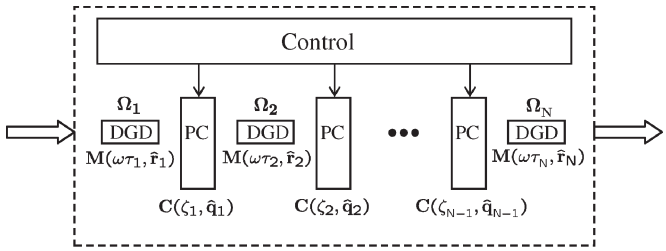

Fig. 1. Schematic illustration of a statistical PMD emulator composed of static-DGD elements separated by randomly driven PCs.

Despite their importance, to date, there has been little published analysis of the impact of artificial cross-channel correlation effects. Related research has instead focused on the single-channel correlation present on fiber links, which has implications for: PMD-induced-pulse distortion [8], [9]; spectrally estimating the mean different group delay (DGD) of a link [10]; and the statistical relationships between different order PMD quantities. One known method to reduce the additional correlation induced by emulators is to increase the number of elements so that each has a smaller individual contribution to the net PMD [11]. However, this is not always practical when size and cost constraints are considered.

Previously, we reported on the interchannel-correlation properties of an emulator design in which the polarization control was provided by rotating the birefringent elements [12]. We presented a simple formula that described the average correlation induced by this emulator design as a weighted sum of the square of the DGDs imparted by each of its constituent elements. The correlation depended upon the relative magnitude and ordering of the section DGDs, both of which can be tailored during the design process. The accuracy of the formula was verified with numerical modeling.

In this paper, we extend our previous result and provide a detailed derivation of a more complete model for the correlation of statistical PMD emulators with symmetric polarization scrambling. We show that average correlation depends on the implementation of the polarization controllers (PCs), and that,

Manuscript received March 30, 2006; revised August 6, 2006. This work was supported by the Australian Research Council (ARC) and National Information and Communication Technology Australia (NICTA), Parkville, VIC 3010, Australia. National ICT Australia is funded by the Australian Government's Backing Australia's Ability initiative, in part through the Australian Research Council.

L. Palmer and J. S. Evans are with the ARC Special Research Centre for Ultrabroadband Information Networks, Department of Electrical and Electronic Engineering, The University of Melbourne, VIC 3010, Australia (e-mail: l.palmer@ee.unimelb.edu.au; j.evans@ee.unimelb.edu.au).

P. M. Farrell and S. D. Dods are with the Victoria Research Laboratory, National ICT Australia, Parkville, VIC 3010, Australia (e-mail: p.farrell@ee.unimelb.edu.au; sarah.dods@nicta.com.au).

Digital Object Identifier 10.1109/JLT.2006.883639

better performance is achieved by increasingly isotropic scrambling. This leads to a possible tradeoff between some simpler PC implementations, such as rotatable connectors [5], and more complicated near-isotropic PC arrangements [13]–[15]. The latter, while having less frequency correlation, may be more susceptible to instability since they are typically constructed by cascading multiple birefringent elements.

II. Statistical PMD Emulators

The class of polarization-scrambled PMD emulators we consider is shown schematically in Fig. 1. The emulators are composed of N-static DGD elements placed in series, with $N-1$ randomly driven PCs positioned between them. For this analysis, we need to consider the PMD vector of each DGD element $\mathbf{\Omega}_k = \tau_k \hat{\mathbf{r}}_k$ [16], where τ_k is the kth element's DGD, and $\hat{\mathbf{r}}_k$ is the principal state of polarization (PSP) and the corresponding Müller matrices $\mathbf{M}_k$ that describe the polarization rotations induced by each element's birefringence. The PCs are represented by their rotation matrices $\mathbf{C}_k$ only, as the PMD they contribute is negligible. The matrices $\mathbf{C}$ and $\mathbf{M}$ have the general rotational form $e^{\zeta(\hat{\mathbf{q}}\times)}$, where the rotation is through an angle ζ counterclockwise about the unit Stokes vector $\hat{\mathbf{q}}$ [17]. The PCs can be configured to have any arbitrary ζ and $\hat{\mathbf{q}}$, while the rotation due to the DGD element has $\zeta = \omega\tau$, and $\hat{\mathbf{q}} = \hat{\mathbf{r}}$, where $\hat{\mathbf{r}}$ corresponds to the fast birefringence axis of the element.

As the most general case, we consider the PCs by their statistical properties. Each PC is characterized by a rotation matrix $\mathbf{C}$. It is a property of such matrices that their columns are the vectors resulting from rotating the Cartesian basis vectors $\hat{\mathbf{s}}_j = (1\ 0\ 0), (0\ 1\ 0)$, and $(0\ 0\ 1)$, respectively, for $j = 1, 2, 3$ [18]. Hence, the matrix elements c_{ij} are the Cartesian components

$$c_{ij} = f_i(\phi_j, \theta_j) = \begin{cases} \cos\phi_j \sin\theta_j, & i = 1 \\ \sin\phi_j \sin\theta_j, & i = 2 \\ \cos\theta_j, & i = 3 \end{cases} \tag{1}$$

where $\phi_j \in [0, 2\pi]$ and $\theta_j \in [0, \pi]$ are the angular spherical coordinates for the rotation of the jth basis vector, illustrated in Fig. 2. We denote the corresponding probability densities for the coordinates by $p(\phi_j)$ and $p(\theta_j)$.

We define a symmetric PC as one that rotates any incident Stokes vector so that its output is symmetrically distributed on the Poincaré sphere. We will show that limiting ourselves to the class of emulators in which the polarization scrambling is symmetric leads to simplifications in the frequency correlation of the device. Using linear superposition, the symmetry condition reduces to the requirement that each of the Cartesian basis vectors has a symmetric output distribution when incident to the PC scrambler. This indicates that $p(\phi_j)$ must be an even function about π over the interval $[0, 2\pi]$ for each j, and $p(\theta_j)$ must be even about $\pi/2$ over $[0, \pi]$.

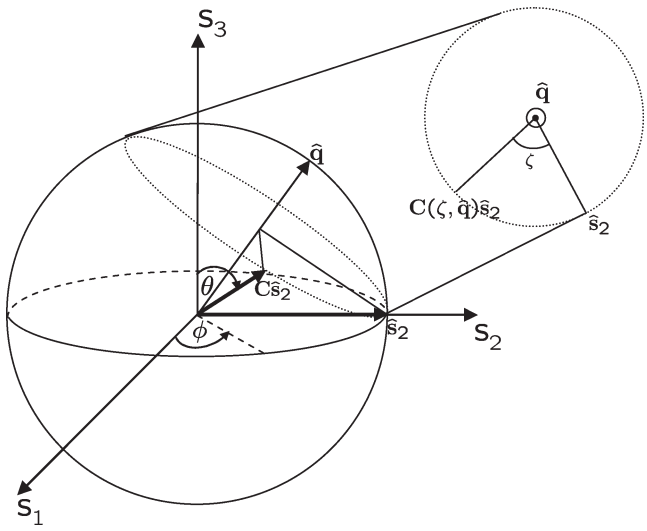

Fig. 2. PCs are characterized by the rotations they apply to Cartesian basis vectors. The rotated unit basis vector is represented by its angular spherical coordinates ($\phi \in [0, 2\pi], \theta \in [0, \pi]$), where the colatitude coordinate θ is subtended from the s_3 axis on the Poincaré sphere.

Lastly, the relationship between the net PMD of an emulator and its constituent elements is known and referred to as the first-order PMD concatenation law [17]. At the output of the link, it is given by

$$\mathbf{\Omega}_{\text{net}}^{\text{out}}(\omega, \xi) = \mathbf{\Omega}_N(\hat{\mathbf{r}}_N) + \sum_{k=1}^{N-1} \mathbf{K}_k^N(\omega, \xi)\mathbf{\Omega}(\hat{\mathbf{r}}_k) \tag{2}$$

where the net vector is the sum of the local PMD vectors rotated into the reference frame of the last element. The matrix $\mathbf{K}_k^N(\omega, \xi)$, shown in (3) at the bottom of the page, where $\mathbb{I}$ is the identity matrix, is the product of element and PC rotations due to successive elements, that is, those with indices greater than k. For example, $\mathbf{K}_1^4 = \mathbf{M}_4\mathbf{C}_3\mathbf{M}_3\mathbf{C}_2\mathbf{M}_2\mathbf{C}_1$. The parameter $\xi \in \mathcal{S}$ represents a polarization scrambling configuration from the set $\mathcal{S}$ of all possible configurations and is itself parameterized by the PC variables ζ_i and $\hat{\mathbf{q}}_i$ for $k \le i \le N$.

III. Background Autocorrelation (BAC)

The discrete structure of concatenated section emulators introduces artificial correlation into the frequency response of the PMD vector. This is in contrast to the situation on a long-fiber link, where the output PMD vector is isotropically distributed on the Poincaré sphere with frequency [19]. As there is no preferred orientation for the vector, the average frequency correlation is zero. However, when an emulator has

$$\mathbf{K}_k^N\left(\omega, \xi(\zeta_k, \ldots, \zeta_{N-1}, \hat{\mathbf{q}}_k, \ldots, \hat{\mathbf{q}}_{N-1})\right) = \begin{cases} \prod_{i=0}^{N-k-1} \mathbf{M}_{N-i}(\omega, \hat{r}_{N-i})\mathbf{C}_{N-i-1}(\zeta_{N-i-1}, \hat{\mathbf{q}}_{N-i-1}), & \text{if } 1 \le k \le N-1 \\ \mathbb{I}, & \text{if } k = N \end{cases} \tag{3}$$

comparatively few elements, the PMD vector is biased so that it is no longer a zero mean process.

The frequency response is quantified by the autocorrelation function (ACF) of the net PMD vector

$$R_{\mathbf{\Omega}}^{\text{out}}(\Delta\omega) = \frac{\left\langle \mathbf{\Omega}^{\text{out}}(\omega_0+\Delta\omega,\xi)\cdot\mathbf{\Omega}^{\text{out}}(\omega_0,\xi)\right\rangle_\xi}{\left\langle \mathbf{\Omega}^{\text{out}}(\omega_0,\xi)\cdot\mathbf{\Omega}^{\text{out}}(\omega_0,\xi)\right\rangle_\xi} \quad (4)$$

where $\Delta\omega$ is an offset from a fixed-optical frequency ω_0. The ensemble expectation is with respect to the polarization scrambling configurations. As the PCs are assumed to be controlled independently, the expectation is separable so that

$$\langle\cdot\rangle_\xi = \langle\cdot\rangle_{\zeta_1,\hat{\mathbf{q}}_1}\langle\cdot\rangle_{\zeta_2,\hat{\mathbf{q}}_2}\cdots\langle\cdot\rangle_{\zeta_{N-1},\hat{\mathbf{q}}_{N-1}}. \quad (5)$$

In the ideal case, where the concatenation of the local PMD vectors closely approximates a Brownian motion [16], the ACF is characterized by a central peak that rapidly and smoothly asymptotes to zero, and has a bandwidth inversely proportional to the mean DGD. The artificial correlation of an emulator manifests as a combination of both nonzero vertical offset in the ACF referred to as the BAC and as oscillatory components. For accurate PMD emulation, the BAC should be low and the oscillatory components damped [2]. Using standard autocorrelation results [20], it can be shown that the BAC is equal to the ratio of the average squared length of the mean PMD vector to its mean-squared length

$$\text{BAC}_{\text{out}} = \frac{\langle\mathbb{E}_\omega\{\mathbf{\Omega}(\omega,\xi)\}\cdot\mathbb{E}_\omega\{\mathbf{\Omega}(\omega,\xi)\}\rangle_\xi}{\langle\mathbb{E}_\omega\{\mathbf{\Omega}(\omega,\xi)\cdot\mathbf{\Omega}(\omega,\xi)\}\rangle_\xi} = 1-\frac{\langle\sigma^2\rangle}{\langle\tau^2\rangle} \quad (6)$$

where $\sigma^2 = \mathbb{E}_{\Delta\omega}\{|\mathbf{\Omega}(\omega,\xi)|^2\} - |\mathbb{E}\{\mathbf{\Omega}(\omega,\xi)\}|^2$ is a variance measure, and $\langle\tau^2\rangle = \langle\mathbb{E}_\omega\{\mathbf{\Omega}(\omega,\xi)\cdot\mathbf{\Omega}(\omega,\xi)\}\rangle_\xi$ is the mean-square DGD. Alternatively, the BAC can be computed directly from the mean of (4) with respect to $\Delta\omega$

$$\begin{aligned}\text{BAC}_{\text{out}} &= \mathbb{E}_{\Delta\omega}\left\{R_{\mathbf{\Omega}}(\Delta\omega)\right\}\\ &= \lim_{W\to\infty}\frac{1}{W}\int_{-\frac{W}{2}}^{\frac{W}{2}} R_{\mathbf{\Omega}}(\Delta\omega)d\Delta\omega. \end{aligned} \quad (7)$$

Over an infinite bandwidth, the central peak has negligible influence in (7), allowing the equation to be used for analysis. However, in practice, for finite-bandwidth simulation and experimental data, the averaging should be performed outside the peak.

One of the consequences of a finite BAC is that the PMD-induced system penalty $\epsilon(\omega)$ associated with different WDM channels becomes correlated. This can be seen from analyzing the mean-square difference in penalties for two arbitrary channels, $\Delta\epsilon = \langle[\epsilon(\mathbf{\Omega}_{\text{Ch1}}) - \epsilon(\mathbf{\Omega}_{\text{Ch2}})]^2\rangle$, which are assumed to be separated by greater than the PMD-vector autocorrelation bandwidth. Expanding the above quadratic gives

$$\langle\Delta\epsilon^2\rangle = \left\langle\epsilon(\mathbf{\Omega}_{\text{Ch1}})^2\right\rangle - 2\left\langle\epsilon(\mathbf{\Omega}_{\text{Ch1}})\epsilon(\mathbf{\Omega}_{\text{Ch2}})\right\rangle + \left\langle\epsilon(\mathbf{\Omega}_{\text{Ch2}})^2\right\rangle. \quad (8)$$

On a real link, the PMD vectors are completely decorrelated outside the autocorrelation bandwidth and thus independent. Therefore, $\langle\epsilon(\mathbf{\Omega}_{\text{Ch1}})\epsilon(\mathbf{\Omega}_{\text{Ch2}})\rangle = \langle\epsilon(\mathbf{\Omega}_{\text{Ch1}})\rangle\langle\epsilon(\mathbf{\Omega}_{\text{Ch2}})\rangle$. Since each channel has the same statistics, the mean-square difference in error penalty between independent channels is twice the variance of the penalty for a single channel

$$\langle\Delta\epsilon^2\rangle = 2\left[\left\langle\epsilon(\mathbf{\Omega})^2\right\rangle - \left\langle\epsilon(\mathbf{\Omega})\right\rangle^2\right]. \quad (9)$$

When the BAC is nonzero, the PMD vectors are frequency correlated, and an incorrect ensemble of penalties is obtained using an emulator.

IV. BAC Model

In this section, we derive an analytical model for describing the BAC for PC-based statistical PMD emulators in terms of their constituent elements. It emerges that if the following constraints are satisfied, the model has a particularly simple form.

1) The emulator elements are linearly birefringent.
2) The polarization rotation due to a PC is uniformly distributed in the output longitudinal component $\phi \in [0, 2\pi]$.
3) The polarization rotation due to a PC is symmetrically distributed about $\pi/2$ in the output colatitude component $\theta \in [0,\pi]$, and $p(\theta_1) = p(\theta_2)$.

Since many practical PC implementations satisfy 1)–3), automatically, the constraints are relatively nonrestrictive.

An overview of the procedure we use to derive the model is as follows. The BAC is first expressed as the sum of N, averaged scalar product terms, $f(\mathbf{\Omega}_k)\cdot g(\mathbf{\Omega}_k)$, where each term is uniquely associated with the PMD vector of each of the N-emulator elements and is a function of the rotations applied by the subsequent elements. The main step of the derivation is to isolate the contribution from the last element and PC, using statistical independence, and then evaluate it. We show that when the PC constraints are applied, the contribution is a scalar multiplicative factor. Using recursion, the contribution from each element is found to be an identical scalar factor, leading to a simple model for the BAC.

We begin by substituting the concatenation law for the emulator (2) into (7). This gives BAC in terms of the PMD vectors of the emulator elements

$$\text{BAC}_{\text{out}} = \frac{1}{\langle\tau^2\rangle}\sum_{k=1}^{N}\sum_{l=1}^{N}\mathbb{E}_{\Delta\omega}\Big\{\left\langle\mathbf{K}_k^N(\omega_0+\Delta\omega,\xi)\mathbf{\Omega}_k\cdot\mathbf{K}_l^N(\omega_0,\xi)\mathbf{\Omega}_l\right\rangle_\xi\Big\}. \quad (10)$$

The expression shows that the BAC is the sum of scalar products between all pairs of rotated local PMD vectors.

Initially, we consider each of the scalar product terms in (10) for which $k \neq l$. Assuming $k > l$ without loss of generality, each term has the unnormalized form

$$\left\langle\mathbb{E}\left\{\mathbf{K}_k^N(\omega_0+\Delta\omega)\mathbf{\Omega}_k\cdot\mathbf{K}_k^N(\omega_0)\mathbf{K}_l^k(\omega_0)\mathbf{\Omega}_l\right\}\right\rangle \quad (11)$$

where $\mathbf{K}_k^N$ is the product of rotations common to both arguments of the scalar product, and $\mathbf{K}_l^k$ contains only those affecting $\mathbf{\Omega}_l$. The PC rotations in $\mathbf{K}_l^k$ occur only once and, using (5), can be replaced by their mean value. In particular,

the matrix adjacent to $\mathbf{\Omega}_l$ is replaced by $\langle \mathbf{C}_l \rangle$, which vanishes when the PC symmetrically rotates any incident polarization. Therefore, the terms for which $k \neq l$ do not contribute to the BAC.

We now consider the product terms for which $k = l$. The contribution from the last section is trivial and equal to $\mathbf{\Omega}_N \cdot \mathbf{\Omega}_N = \tau_N^2$. The remaining terms, when $k < N$, can be represented as

$$\chi_k = \big\langle \mathbb{E}\big\{ \mathbf{\Omega}_k^{\mathrm{T}} (\mathbf{K}_k^{N-1}(\omega_0 + \Delta\omega)^{\mathrm{T}} \mathbf{C}_{N-1}^{\mathrm{T}} \mathbf{M}_N^{\mathrm{T}}(\omega_0 + \Delta\omega) \times \mathbf{M}_N(\omega_0) \mathbf{C}_{N-1} \mathbf{K}_k^{N-1}(\omega_0) \mathbf{\Omega}_k \big\} \big\rangle \quad (12)$$

where the matrices associated with the last emulator element and PC have been extracted from $\mathbf{K}_k^N$ and were shown explicitly in preparation for evaluating each element's contribution separately. Therefore, a simplified expression for the BAC containing only $k = l$ scalar product terms is

$$\mathrm{BAC}_{\mathrm{out}} = \frac{1}{\langle \tau^2 \rangle} \sum_{k=1}^{N} \chi_k. \quad (13)$$

The aim of the next step is to find a simple closed-form expression for each χ_k by separating out the contributions from the element and PC rotations using statistical independence.

We first note that since each χ_k evaluates to a scalar, a trace operator may be applied to (12) without affecting the overall result. The order of multiplication of the rotations can be rearranged using trace-permutation properties to aid in separating the expectation operators and recursively finding a simpler expression. Using PC independence, each pair of $\mathbf{C}_k$ terms with the same index may be separated from each other pair. Furthermore, assuming the static-DGD elements have random DGDs, the rotation angles of the $\mathbf{M}_k$ are linear functions of frequency with random slopes. Therefore, over an infinite $\Delta\omega$ interval, differently subscripted pairs of $\mathbf{M}_k$ are also separable with respect to $\mathbb{E}_{\Delta\omega}\{\cdot\}$.

We proceed by setting $\mathbf{A} = \mathbf{\Omega}_k^{\mathrm{T}} (\mathbf{K}_k^{N-1}(\omega_0 + \Delta\omega)^{\mathrm{T}}$ and $\mathbf{B} = \mathbf{C}_{N-1}^{\mathrm{T}} \mathbf{M}_N^{\mathrm{T}}(\omega_0 + \Delta\omega) \mathbf{M}_N(\omega_0) \mathbf{C}_{N-1} \mathbf{K}_k^{N-1}(\omega_0) \mathbf{\Omega}_k$, and using $\mathrm{Tr}[\mathbf{AB}] = \mathrm{Tr}[\mathbf{BA}]$, so that χ_k becomes

$$\chi_k = \mathrm{Tr}\Bigg[\Big\langle \mathbf{C}_{N-1}^{\mathrm{T}} \mathbb{E}\big\{ \mathbf{M}_N^{\mathrm{T}}(\omega_0 + \Delta\omega) \big\} \mathbf{M}_N(\omega_0) \mathbf{C}_{N-1} \Big\rangle \times \Big\langle \mathbf{K}_k^{N-1}(\omega_0) \mathbf{\Omega}_k \mathbf{\Omega}_k^{\mathrm{T}} \mathbb{E}\Big\{ \big(\mathbf{K}_k^{N-1}\big)^{\mathrm{T}} (\omega_0 + \Delta_\omega) \Big\} \Big\rangle \Bigg]. \quad (14)$$

By permuting the trace as described, the rotations associated with the last element and PC have been brought to the left of the expression, allowing the ensemble expectation to be separated. The left-hand expectation reduces to

$$\mathbf{\Lambda} = \big\langle \mathbf{C}_{N-1}^{\mathrm{T}}(\zeta_{N-1}, \hat{q}_{N-1}) \mathbb{E}_{\Delta\omega} \{ \mathbf{M}_N(\Delta\omega, \hat{r}_N) \} \cdot \mathbf{C}_{N-1}(\zeta_{k-1}, \hat{q}_{N-1}) \big\rangle \quad (15)$$

where the properties $\mathbf{M}^{\mathrm{T}}(\zeta, \hat{r}) = \mathbf{M}^{-1} T(\zeta, \hat{r}) = \mathbf{M}(-\zeta, \hat{r})$, and $\mathbf{M}(\zeta_1, \hat{r}) \mathbf{M}(\zeta_2, \hat{r}) = \mathbf{M}(\zeta_1 + \zeta_2, \hat{r})$ for rotation matrices with the same rotation axes have been used to simplify the expression.

In order to simplify $\mathbf{\Lambda}$, we apply the following symmetry constraints. In simple notation $\mathbf{\Lambda} = \langle \mathbf{C}^{\mathrm{T}} \mathbf{R} \mathbf{C} \rangle$, where

$$\mathbf{R} = \mathbb{E}\{ \mathbf{M}(\omega, \hat{\mathbf{r}}) \} = \begin{pmatrix} r_1^2 & r_1 r_2 & r_1 r_3 \\ r_2 r_1 & r_2^2 & r_2 r_3 \\ r_3 r_1 & r_3 r_2 & r_3^2 \end{pmatrix} \quad (16)$$

is a symmetric matrix with $\hat{\mathbf{r}} = (r_1\ r_2\ r_3)$. A direct expansion of $\mathbf{\Lambda}$ yields components with the form

$$\Lambda_{ij} = \sum_{k=1}^{3} \sum_{l=1}^{3} \langle c_{ki} c_{lj} \rangle r_k r_l. \quad (17)$$

When the symmetry constraints are applied, $\mathbf{\Lambda}$ reduces to a diagonal matrix. To see this, we consider separately each of the four possible combinations of i, j, k, and l.

Case 1) $i = k$, $j = l$: The mean-square components of the rotated basis vectors are given by

$$\big\langle c_{ij}^2 \big\rangle = \int_0^{\pi} \int_0^{2\pi} f_i^2(\phi_j, \theta_j) p(\phi_j, \theta_j) d\phi_j d\theta_j \neq 0. \quad (18)$$

Importantly, these terms are nonzero.

Case 2) $i = k$, $j \neq l$: The mean products of the same component of different rotated basis vectors are given by

$$\langle c_{ij} c_{il} \rangle = \int_0^{\pi} \int_0^{2\pi} \int_0^{\pi} \int_0^{2\pi} f_i(\phi_j, \theta_j) f_i(\phi_l, \theta_l) p(\phi_j, \theta_j, \phi_l, \theta_l) \cdot d\phi_j d\theta_j d\phi_l d\theta_l. \quad (19)$$

Using Bayes rule, $p(\phi_j, \theta_j, \phi_l, \theta_l) = p(\phi_l, \theta_l) p \times (\phi_j, \theta_j | \phi_l, \theta_l)$. Since each $f_i(\phi, \theta)$ is an odd function over the intervals of the independent variables, $\langle c_{ij} c_{il} \rangle = 0$ if $p(\phi_l, \theta_l)$, and $p(\phi_j, \theta_j | \phi_l, \theta_l)$ are both even functions. From PC symmetry constraints, $p(\phi_j, \theta_j)$ and $p(\phi_l, \theta_l)$ are both even functions. It follows that $p(\phi_j, \theta_j | \phi_l, \theta_l)$ is also even, since geometrically it is the intersection of $p(\phi_j, \theta_j)$ with a plane passing through the origin, which preserves symmetry.

Case 3) $i \neq k$, $j = l$: The mean products of different components of the same rotated basis vector are given by

$$\langle c_{ij} c_{kj} \rangle = \int_0^{\pi} \int_0^{2\pi} f_i(\phi_j, \theta_j) f_k(\phi_j, \theta_j) p(\phi_j, \theta_j) d\phi_j d\theta_j. \quad (20)$$

Each $f_i(\phi_j, \theta_j) f_k(\phi_j, \theta_j)$ product is an odd function for $i \neq k$. Therefore, $\langle c_{ij} c_{kj} \rangle = 0$, since $p(\phi_j, \phi_j)$ is an even function.

Case 4) $i \neq k$, $j \neq l$: The mean products of different components of different rotated basis vectors are given by

$$\langle c_{ij}c_{kl}\rangle = \int_0^{\pi}\int_0^{2\pi}\int_0^{\pi}\int_0^{2\pi} f_i(\phi_j,\theta_j)f_k(\phi_l,\theta_l)p(\phi_j,\theta_j,\phi_l,\theta_l) \cdot d\phi_j d\theta_j d\phi_l d\theta_l. \quad (21)$$

For each of the three combinations of $f_i(\cdot)f_k(\cdot)$ and $i \neq k$, there exists at least one variable for which the integrand is odd with respect to the integrating variable. Thus, $\langle c_{ij}c_{kl}\rangle = 0$, when $p(\phi_j,\theta_j,\phi_l,\theta_l)$ is an even function with respect to that variable. Symmetry again ensures that this will be the case.

Applying the above results, the final expression for $\mathbf{\Lambda}$ is

$$\mathbf{\Lambda} = \begin{pmatrix} \sum_{i=1}^{3}\langle c_{i1}^2\rangle r_i^2 & 0 & 0 \\ 0 & \sum_{i=1}^{3}\langle c_{i2}^2\rangle r_i^2 & 0 \\ 0 & 0 & \sum_{i=1}^{3}\langle c_{i3}^2\rangle r_i^2 \end{pmatrix} \quad (22)$$

which is diagonal and can be computed from (18) for any arbitrarily implemented PC that satisfies the symmetry constraints. This includes simple randomly driven configurations of waveplates and phaseplates, for which the probability densities can be computed analytically or numerically for each basis vector or more advanced PCs driven by software algorithms.

The final step of the derivation is to use recursion to find the total contribution from χ_k after multiple rotations are applied. From our previous analysis, (14) can now be simplified to

$$\chi_k = \mathrm{Tr}\left[\mathbf{\Lambda}\left\langle \mathbf{K}_k^{N-1}(\omega_0)\mathbf{\Omega}_k\mathbf{\Omega}_k^{\mathrm{T}}\mathbb{E}\left\{\left(\mathbf{K}_k^{N-1}\right)^{\mathrm{T}}(\omega_0+\Delta_\omega)\right\}\right\rangle\right] \quad (23)$$

where $\mathbf{\Lambda}$ is the contribution from the last emulator element and PC. A clockwise cyclic permutation to the trace argument resets the algorithm so that

$$\chi_k = \mathrm{Tr}\Big[\left\langle \mathbf{C}_{N-2}^{\mathrm{T}}\mathbb{E}\left\{\mathbf{M}_{N-1}^{\mathrm{T}}(\omega_0+\Delta\omega)\right\}\mathbf{\Lambda}\mathbf{M}_{N-1}(\omega_0)\mathbf{C}_{N-2}\right\rangle \times\left\langle \mathbf{K}_k^{N-2}(\omega_0)\mathbf{\Omega}_k\mathbf{\Omega}_k^{\mathrm{T}}\mathbb{E}\left\{\left(\mathbf{K}_{k+1}^{N-2}\right)^{\mathrm{T}}(\omega_0+\Delta_\omega)\right\}\right\rangle\Big] \quad (24)$$

where, now, the matrices associated with the second to last emulator element and PC have been extracted from $\mathbf{K}_k^{N-1}$, just as $\mathbf{M}_N$ and $\mathbf{C}_{N-1}$ were in the first iteration of the algorithm.

The contribution, due to the last two pairs of rotations, is $\langle \mathbf{C}_{N-2}^{\mathrm{T}}\mathbb{E}\{\mathbf{M}_{N-1}^{\mathrm{T}}(\omega_0+\Delta\omega)\}\mathbf{\Lambda}\mathbf{M}_{N-1}(\omega_0)\mathbf{C}_{N-2}\rangle$. The PC symmetry constraints cause $\mathbf{\Lambda}$ to be diagonal. However, $\mathbf{\Lambda}$ can be further simplified if the following constraints are met: The emulator elements are also linearly birefringent; $p(\phi_i)$ is uniform for each basis vector; and $p(\theta_1) = p(\theta_2)$. Linearly birefringent elements constrain the rotation axes of the elements to the equator of the Poincaré sphere so that $r_3 = 0$ in (16) and (17). It follows that the third element of the corresponding local PMD vector must also be zero since it defines the rotation axis. Using this additional constraint

$$\mathbf{\Lambda} = \begin{pmatrix} \langle c_{11}^2\rangle r_1^2 + \langle c_{21}^2\rangle r_2^2 & 0 & 0 \\ 0 & \langle c_{12}^2\rangle r_1^2 + \langle c_{22}^2\rangle r_2^2 & 0 \\ 0 & 0 & \langle c_{13}^2\rangle r_1^2 + \langle c_{23}^2\rangle r_2^2 \end{pmatrix}. \quad (25)$$

The second and third sets of conditions lead to the upper two diagonal elements of $\mathbf{\Lambda}$ being the same. Combining (1) and (18)

$$\langle c_{1i}^2\rangle = \int_0^{2\pi}\cos^2\phi_i p(\phi_i)d\phi_i \int_0^{\pi}\sin^2\theta_i p(\theta_i)d\theta_i = \kappa_i\rho_i \quad (26)$$

$$\langle c_{2i}^2\rangle = \int_0^{2\pi}\sin^2\phi_i p(\phi_i)d\phi_i \int_0^{\pi}\sin^2\theta_i p(\theta_i)d\theta_i = (1-\kappa_i)\rho_i \quad (27)$$

where κ corresponds to the ϕ integral and ρ the θ integral. For a uniformly distributed ϕ_i, $p(\phi_i) = 1/2\pi$, and $\kappa_i = 1/2$ for $i = 1,2,3$; while $p(\theta_1) = p(\theta_2)$ gives $\rho_1 = \rho_2$. Combining with the norm identity $r_1^2 + r_2^2 = 1$, $\mathbf{\Lambda}$ becomes

$$\mathbf{\Lambda} = \begin{pmatrix} \frac{1}{2}\rho_1 & 0 & 0 \\ 0 & \frac{1}{2}\rho_1 & 0 \\ 0 & 0 & \frac{1}{2}\rho_3 \end{pmatrix} = \frac{1}{2}\rho_1\mathbb{I} - \mu\mathbf{X} \quad (28)$$

where

$$\mu = \frac{\rho_1(\rho_1-\rho_3)}{2} \quad (29)$$

and

$$\mathbf{X} = \begin{pmatrix} 0 & 0 & 0 \\ 0 & 0 & 0 \\ 0 & 0 & 1 \end{pmatrix}. \quad (30)$$

Substituting (28) into (23) and using the additive properties of traces, χ_k becomes

$$\chi_k = \frac{\rho_1}{2}\mathrm{Tr}\left[\left\langle \mathbf{K}_k^{N-1}(\omega_0)\mathbf{\Omega}_k\mathbf{\Omega}_k^{\mathrm{T}}\mathbb{E}\left\{\left(\mathbf{K}_k^{N-1}\right)^{\mathrm{T}}(\omega_0+\Delta_\omega)\right\}\right\rangle\right] - \mu\mathrm{Tr}\left[\mathbf{X}\left\langle \mathbf{K}_k^{N-1}(\omega_0)\mathbf{\Omega}_k\mathbf{\Omega}_k^{\mathrm{T}}\mathbb{E}\left\{\left(\mathbf{K}_k^{N-1}\right)^{\mathrm{T}}(\omega_0+\Delta_\omega)\right\}\right\rangle\right]. \quad (31)$$

However, the second trace is zero. This can be seen by permuting the argument so that $\mathbf{X}$ is on the right and moving it inside the expectation. $\mathbf{X}$ now multiplies $\mathbb{E}\{\mathbf{M}_i(\omega_0+\Delta\omega)\}$. Since $r_3 = 0$, the product has the special form

$$\left[\begin{array}{c|c} \mathbf{A} & 0 \\ \hline 0 & 0 \end{array}\right]\left[\begin{array}{c|c} 0 & 0 \\ \hline 0 & 1 \end{array}\right] = 0 \quad (32)$$

where $\mathbf{A}$ is the upper left 2×2 submatrix of (16). Thus, only the first term in (31) contributes. Specifically, it introduces a scalar factor of $\rho_1/2$, and the identity matrix is absorbed. After further trace permutation, a reduced expression for (23) is then

$$\chi_k = \frac{\rho_1}{2}\mathrm{Tr}\left[\left\langle \mathbf{\Omega}_k^{\mathrm{T}}\mathbb{E}\left\{\left(\mathbf{K}_k^{N-1}\right)^{\mathrm{T}}(\omega_0+\Delta_\omega)\right\}\mathbf{K}_k^{N-1}(\omega_0)\mathbf{\Omega}_k\right\rangle\right]. \quad (33)$$

This equation has the same form as the original problem except with one less pair of matrices. Therefore, the procedure described above can be repeatedly applied to remove each pair of matrices with the same index. Each stage of the iterative algorithm introduces a factor of a $(\rho_1/2)\mathbb{I}$, and the contribution from the kth emulator element term is

$$\chi_k = \left(\frac{\rho_1}{2}\right)^{N-k} \left\langle \vec{\Omega}_j^{\mathrm{T}} \vec{\Omega}_k \right\rangle = \left(\frac{\rho_1}{2}\right)^{N-k} \tau_k^2. \tag{34}$$

Combining the above results, a general formula is found for the BAC of polarization scrambled statistical PMD emulators employing linearly birefringent elements and PCs that: 1) uniformly randomize the longitudinal angle of each rotated basis vector; 2) symmetrically rotate the colatitude angle of each rotated basis vector; and 3) have identical colatitude distributions for the rotated $\hat{s}_1$ and $\hat{s}_2$ basis vectors

$$\mathrm{BAC}_{\mathrm{out}} = \frac{\sum_{k=1}^{N} \beta^{N-k} \tau_k^2}{\sum_{k=1}^{N} \tau_k^2}. \tag{35}$$

We refer to $\beta = \rho_1/2$ as the base weight factor. Equation (35) is the main result of this paper. It links the BAC of an emulator to parameters describing its discretization relative to an actual fiber, which is the number of elements, their size (DGD), and their relative ordering.

V. Model Analysis

In this section, we show how the derived BAC relationship can be applied to several common PC implementations.

A. Rotatable Element Emulator

The rotatable-element-emulator design is widely used due to its simple control and relative robustness. It includes birefringent crystals cascaded in rotatable mounts, as well as polarization maintaining (PM) fiber sections combined in series with rotatable connectors. The emulator fits within the PC framework shown in Fig. 1, since a rotatable linearly birefringent element can be equivalently modeled by a fixed element sandwiched between two rotations about the s_3 axis with opposite angles

$$\mathbf{M}_k\left(\omega\tau_k, \hat{\mathbf{r}}(\phi_k)\right) \equiv \mathbf{C}_{s_3}\left(-\phi_k, \hat{\mathbf{s}}_3\right)) \mathbf{M}_k(\omega\tau_k, \mathbf{0}) \mathbf{C}_{s_3}(\phi_k, \hat{\mathbf{s}}_3)) \tag{36}$$

as shown in Fig. 3. The PC between the kth and $(k+1)$th elements is replaced by the rotation product $\mathbf{C}_{s_3}(\phi_k)\mathbf{C}_{s_3}(-\phi_{k+1}) = \mathbf{C}_{s_3}(\phi_k - \phi_{k+1})$. As each ϕ_k is independently driven uniformly randomly, the emulator effectively consists of static DGD elements separated by independent uniformly rotations about the s_3 axis over the interval $[0, 2\pi]$.

To derive the BAC model for this emulator type, we need to determine the probability densities of the PCs when operated on the Cartesian basis vectors. In this case, the PCs uniformly randomize the $\mathbf{s}_1$ and $\mathbf{s}_2$ basis vectors on the equator of the Poincaré sphere so that $p(\phi_{1,2}) = 1/2\pi$, $p(\theta_{1,2}) = \delta(\theta_{1,2} - \pi/2)$, and $\mathbf{s}_3$ is unaffected. Evaluating (26) and (27), $\kappa_{1,2,3} = 1/2$, $\rho_1 = \rho_2 = 1/2$, and $\rho_3 = 0$. Substituting these values into (28), $\mathbf{\Lambda}$ becomes

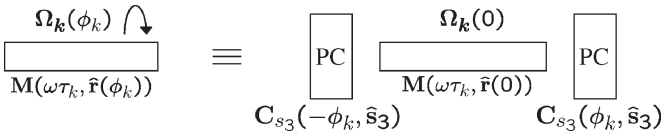

Fig. 3. Rotatable linearly birefringent element is equivalent to a fixed element sandwiched between two rotations about the s_3 Stokes axis, with angles equal to plus and minus the orientation of the element's birefringence axis.

$$\mathbf{\Lambda} = \begin{pmatrix} \frac{1}{2} & 0 & 0 \\ 0 & \frac{1}{2} & 0 \\ 0 & 0 & 0 \end{pmatrix} \tag{37}$$

and the BAC, with respect to the output PMD vector, is given by

$$\mathrm{BAC}_{\mathrm{out}} = \frac{\sum_{k=1}^{N} \left(\frac{1}{2}\right)^{N-k} \tau_k^2}{\sum_{k=1}^{N} \tau_k^2}. \tag{38}$$

The base weight factor for the BAC model for rotatable connectors is therefore 1/2. This is the result we previously presented in [12].

B. Rotatable Quarter-Half-Quarter (QHQ) Waveplates

Next, we consider an emulator where the PCs are implemented in the commonly employed rotatable QHQ-waveplate configuration. The matrix $\mathbf{C}(\zeta, \hat{\mathbf{q}})$ is equal to $\mathbf{C}_{1/4}(\pi/2, \hat{\mathbf{r}}(\phi_3))\mathbf{C}_{1/2}(\pi, \hat{\mathbf{r}}(\phi_2))\mathbf{C}_{1/4}(\pi/2, \hat{\mathbf{r}}(\phi_1))$, where $\hat{\mathbf{r}}(\phi_{1,2,3})$ are independent rotation axes on the equator of the Poincaré esphere. We determined the probability density functions for each of the basis vector rotations numerically and used them to evaluate (26) and (27). We found that $\kappa_{1,2,3} = 1/2$, $\rho_{1,2} = 3/4$, and $\rho_3 = 1/2$. Combining, $\mathbf{\Lambda}$ is given by

$$\mathbf{\Lambda} = \begin{pmatrix} \frac{3}{8} & 0 & 0 \\ 0 & \frac{3}{8} & 0 \\ 0 & 0 & \frac{1}{4} \end{pmatrix} \tag{39}$$

and the BAC by

$$\mathrm{BAC}_{\mathrm{out}} = \frac{\sum_{k=1}^{N} \left(\frac{3}{8}\right)^{N-k} \tau_k^2}{\sum_{k=1}^{N} \tau_k^2}. \tag{40}$$

The base weight factor for the BAC model for QHQ polarization scrambling is therefore 3/8.

C. Isotropic Polarization Scrambling

Isotropic polarization scrambling between static-DGD elements is closely related to the rotatable-element-emulator case. Where the latter uniformly randomizes the polarization in the equatorial plane, isotropic scrambling randomizes in three dimensions, providing uniform coverage of the Poincaré esphere. This model is typically used to represent fibers or emulators in simulations, for example, by Karlsson and Brentel [8], when deriving the ACF of an ideal link. To analyze the emulator, we assume that there exists some PC implementation

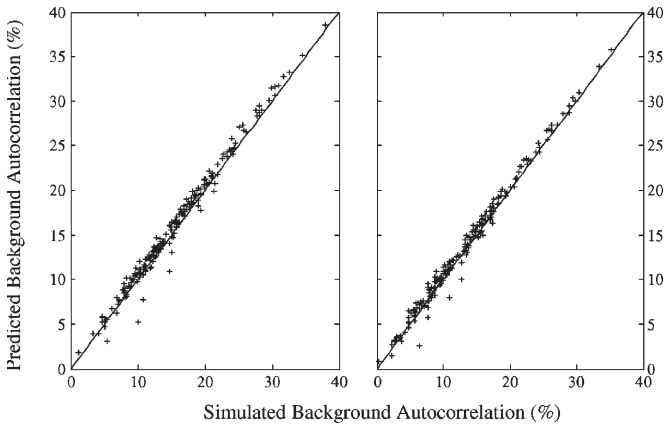

Fig. 4. Simulation comparison of 15-section emulator designs using rotatable connectors (left) and cascaded QHQ-waveplate PCs (right) with the derived BAC model.

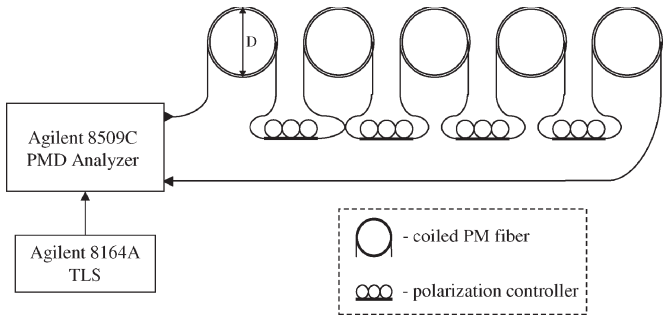

Fig. 5. Experimental setup for testing the BAC model for an emulator with QHQ-waveplate-PC scrambling using PM-fiber elements. The coil diameter D of the fiber is 20 cm.

that isotropically randomizes the three Cartesian basis vector. From standard spherical-geometry results, isotropy requires that $p(\phi_{1,2,3}) = 1/2\pi$, and $p(\theta_{1,2,3}) = (1/2)\sin(\theta_{1,2,3})$. Evaluating (26) and (27), and substituting into (28) gives $\mathbf{\Lambda}$ for the isotropic scrambling case as

$$\mathbf{\Lambda} = \begin{pmatrix} \frac{1}{3} & 0 & 0 \\ 0 & \frac{1}{3} & 0 \\ 0 & 0 & \frac{1}{3} \end{pmatrix}. \tag{41}$$

The base weight factor for the BAC model for the emulator with isotropic polarization scrambling is therefore 1/3, which differs from the QHQ case by just 1/24.

VI. Model Verification

We investigated the validity of the BAC models for the rotatable element and QHQ-waveplate emulators by performing Monte Carlo simulations using Jones matrix eigenanalysis [22], and comparing the simulated BACs with those predicted by the models shown in (38) and (40). The static-DGD elements were generated with random-fixed orientations, and the polarization scramblers between elements in the QHQ case were modeled by three rotatable waveplates. We simulated 200 15-section emulators with different element DGDs. The DGDs were randomly selected to be 20% Gaussian distributed and produce rms DGDs of 40 ps. There were 2000 independent random-coupling configurations generated and the PMD vectors determined for each of 201 equally spaced frequencies in a 2-THz bandwidth. For each emulator, we computed the output-PMD-frequency ACFs for every selected set of PC setting. The BAC for each DGD configuration was estimated from the average ACF outside the central peak. Fig. 4 shows adjacent plots of the predicted versus estimated BAC for the rotatable element and QHQ emulators. Excellent agreement is found for the simulation and analytical model. The few anomalous points can be associated with unbalanced constructive interference of oscillatory components over the finite-ACF-frequency range. A nonlinear least square-parameter estimate [23] for the base weight factor gives 0.4795 ± 0.005 for the rotatable-element emulator, compared with the expected value of 0.5, and 0.3446 ± 0.006 for the QHQ emulator, compared with the expected value of 0.375. We believe that the slight underestimation of the parameter in both cases is, again, due to localized periodic features over the ACF frequency range.

We also investigated the QHQ model experimentally by constructing a five-section emulator with three-paddle PCs between sections of PM fiber. The experimental setup is shown in Fig. 5. The emulator was placed between the input and output ports of an Agilent 8509C Lightwave polarization analyzer, which had a continuous-wave optical signal supplied to it by an Agilent 8194A tunable laser source. The PM fiber used in the emulator had a nominal-beat length of 3.02 mm at 1550 nm, which corresponds to a DGD of 1.7 ps/m. The ends of the fiber were spliced to single-mode-fiber pigtails for straightforward connection to the PCs and reordering of the sections. Each PM section was insulated from ambient, thermal, and vibrational effects sufficiently that the output polarization was stable on the order of 5–10 min, which was greater than the time required to obtain the PMD-frequency response for a single nominally stable PC setting. The rms DGD of the emulator was 19 ps, and the section DGDs 13.75, 6.76, 9.08, 5.21, and 3.87 ps. Four permutations of the section ordering were investigated to generate a spread of BAC values.

The emulator ACFs were determined at 51 equally spaced frequencies in a 400-GHz bandwidth centered at 1550 nm. The ACF at each frequency was computed from (4) using an ensemble of PMD-vector measurements corresponding to 30 randomly selected PC settings. Since the polarization analyzer uses mechanically controlled optics, and the mode coupling configurations are set manually, we found it necessary to minimize the number of measured data points in order to ensure realistic running times for the experiment. While quite small, we found that an ensemble of just 30-mode coupling configurations was sufficient to compute BACs that approximately matched the model predictions to within experimental error. Simulations verified that BACs computed using these many configurations were within a few percent of those obtained using 2000 configurations (the number used to generate each point in Fig. 4).

The experimental BACs we obtained for four different permutations of section ordering and their corresponding model predictions are shown in Fig. 6 and illustrate reasonably good agreement. The error bars correspond to 95% confidence intervals computed assuming Gaussian statistics. A least square-parameter estimation of the four points gives a base weight factor of 0.39 ± 0.126, which is quite close to the expected

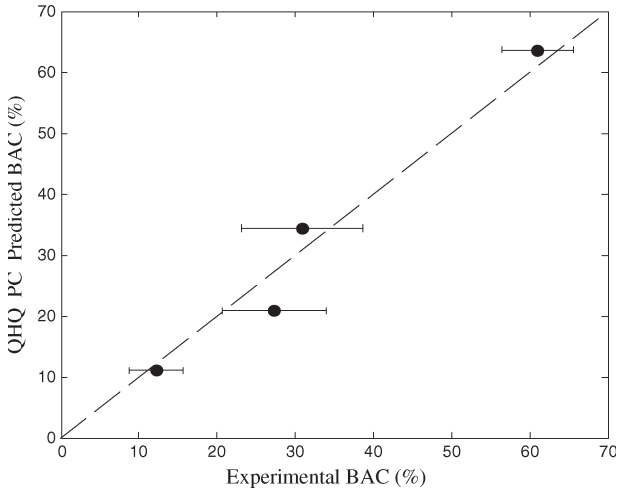

Fig. 6. Experimental comparison with the derived BAC model of a five-section polarization scrambled PMD emulator using cascaded QHQ-retarder fiber paddle PCs.

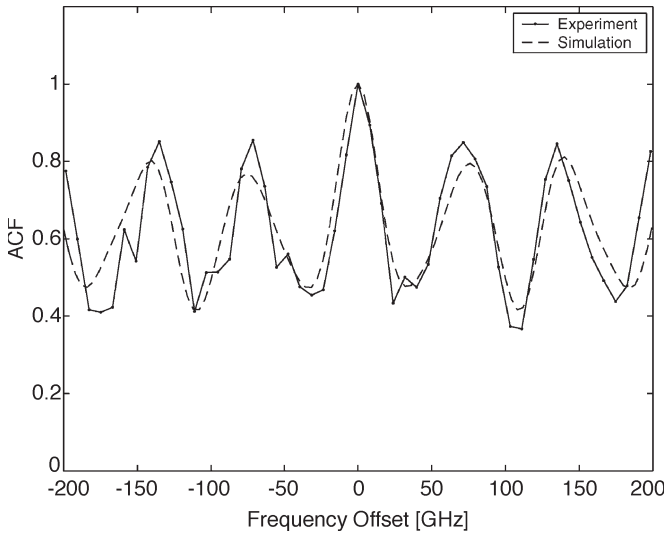

Fig. 7. Experimental and simulation comparison of the ACF for a five-section polarization scrambled PMD emulator using QHQ-retarder PC scrambling.

0.375. However, the 95% confidence interval is quite large since the graph contains only four points. Fig. 7 shows an example of the relatively close matching between experimental and simulated ACF we were able to obtain for one ordering of section DGDs. The strong periodicity is due to the emulator containing only five sections.

VII. Discussion

We have developed a model that links the BAC of an emulator to the ordering of its elements. First, the model illustrates that the BAC is reduced when the polarization scrambling is close to isotropic. Second, it illustrates that placing elements with lower DGDs near the end minimizes the output BAC.

One issue to consider is whether the DGD of the last element of an emulator can be decreased arbitrarily close to zero, thereby reducing the output BAC, and the model still remains valid. For an emulator with a fixed number of elements to maintain a constant mean DGD, the other element's DGDs must be correspondingly increased. By decreasing the last element's DGD, the rate at which it causes an incident signals' polarization to rotate is similarly reduced. In the limit of a small DGD compared to the other elements, it ceases to have any appreciable effect over the bandwidth of the system, and the emulator behaves as if it had one fewer element. Determining an analytic description for this phenomena is a focus for future work.

The second issue to consider is the interpretation of the BAC, given that it is derived in a specific reference frame. The concatenation law in (2) is for the output PMD vector, but it is just as valid to describe a system's PMD by the frequency dependence of the input PMD vector $\mathbf{\Omega}_{\rm in} = \widetilde{\mathbf{M}}^{-1}(\omega)\mathbf{\Omega}_{\rm out}$, where $\widetilde{\mathbf{M}}(\omega)$ is the net Müller matrix describing the polarization transformation due to birefringence. It is straightforward to show, by considering light propagating in the opposite direction through the cascaded birefringent elements, that the analysis proceeds almost exactly as before but with the indices reversed and the Müller matrices transposed. Following this argument, the BAC at the input is given by

$$\mathrm{BAC}_{\rm in} = \frac{\sum_{k=1}^{N} \beta^{k-1} \tau_k^2}{\sum_{k=1}^{N} \tau_k^2}. \tag{42}$$

The above analysis illustrates that by ordering the elements from largest DGD to smallest, an emulator can be constructed with low-output BAC and high-input BAC or by reversing the ordering, high-output BAC, and low-input BAC. Similarly, by locating the larger DGD elements in the center, the BAC can be reduced at both the input and output to a degree. The PMD vector ACF has been shown to be the product of the ACF of the DGD and the ACF of the PSP, with the latter dominating [8]. Therefore, the BAC in the input and output frames directly corresponds to the degree of correlation of the corresponding input and output PSPs.

From a practical perspective, decorrelated-input PSPs may be required when a system under test employs PSP launch alignment at the transmitter to mitigate PMD. Similarly, decorrelated-output PSPs may be necessary to properly test a PMD compensator that simultaneously compensates multiple WDM channels. It is an open question, however, whether designing for low input and output BAC for a fixed number of elements provides overall reduction in the interchannel correlation. It appears that moving the higher DGD elements closer to the center of the emulator merely localizes the positions of correlated PSPs away from the input and output, but may not offer any overall improvement. Instead, fundamental improvement is gained by either improving the isotropy of the polarization rotations, which converges to a hard limit and offers only modest improvement, or by increasing the number of elements.

Last, it is possible to extend the BAC model to a more advanced PMD-emulator designs constructed with variable DGD elements [24], [25]. Assuming mutual independence between the element DGDs, as well as dynamic polarization scrambling between them, the BAC for the variable DGD emulator is given by the slightly modified formula

$$\mathrm{BAC}_{\rm out} = \frac{\sum_{k=1}^{N} \beta^{N-k} \left\langle \tau_k^2 \right\rangle}{\sum_{k=1}^{N} \left\langle \tau_k^2 \right\rangle} \tag{43}$$

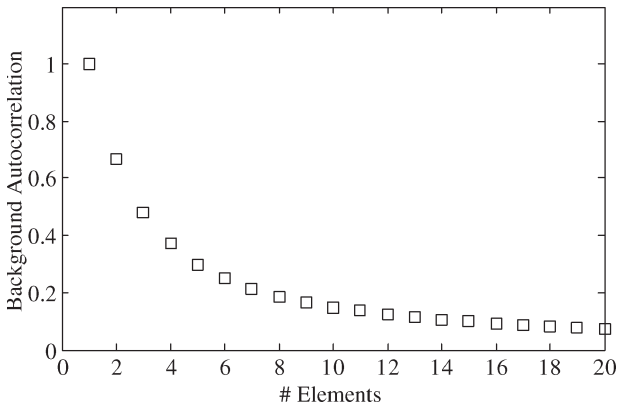

Fig. 8. BAC versus number of elements for a variable DGD-PMD emulator with mean DGD of 50 ps.

where the expectation is with respect to the element DGD statistics. One verification of the formula is found by comparing it with the Monte Carlo-based analysis reported in [25] for an emulator design in which the element DGDs are independently and identically distributed (i.i.d) Maxwellian random variables. The concatenation of Maxwellian DGD elements results in a similarly Maxwellian net DGD [26], which obeys

$$\langle \tau^2 \rangle = \sum_{k=1}^{N} \langle \tau_k^2 \rangle = N \langle \tau_0^2 \rangle \tag{44}$$

where $\langle \tau^2 \rangle$ is the desired net mean-square DGD, and $\tau_k = \tau_0$ are the i.i.d element DGDs. Thus, the individual element mean-square DGDs are equal to the net mean-square DGD divided by the number of elements. Setting the mean DGD to 50 ps and assuming perfect isotropic polarization scrambling as in [25], the relationship between the BAC and the number of emulator elements is obtained using (43), as shown in Fig. 8. Comparing this graph with [25, Fig. 5(b)] they are almost indistinguishable, illustrating the strong correlation between theory and independent simulation.

VIII. Conclusion

We have rigorously derived a model for the BAC of statistical PMD emulators with symmetric polarization scrambling. The model illustrates that the average PMD-vector frequency correlation depends on the number of emulator elements, their relative DGDs and ordering, and the isotropy of the polarization scrambling. Increasing the number of elements and PC isotropy improves the BAC in an absolute sense, while ordering the elements can minimize the PSP correlation at the input, output, or jointly, which is useful for testing different types of broadband-PMD-mitigation techniques. The effects of highly localized BAC within the emulator on WDM PMD emulation are unclear at this stage.

References

[1] D. Breuer, H.-J. Tessmann, A. Gladisch, H. Foisel, G. Neumann, H. Reiner, and H. Cremer, "Measurements of PMD in the installed fiber plant of Deutsche Telekom," presented at the Digest of Holey Fibers and Photonic Crystals/Polarization Mode Dispersion/Photonics Time/Frequency Measurement and Control, LEOS Summer Topical Meetings, Vancouver, BC, Canada, 2003, Paper MB2.1.

[2] J. Lima, I. T. R. Khosravani, P. Ebrahimi, E. Ibragimov, C. R. Menyuk, and A. E. Willner, "Comparison of polarization mode dispersion emulators," *J. Lightw. Technol.*, vol. 19, no. 12, pp. 1872–1881, Dec. 2001.

[3] J. N. Damask, "Methods to construct programmable PMD sources—Part I: Technology and theory," *J. Lightw. Technol.*, vol. 22, no. 4, pp. 997–1005, Apr. 2004.

[4] M. C. Hauer, Q. Yu, A. E. Willner, E. R. Lyons, C. H. Lin, A. A. Au, and H. P. Lee, "Compact, all-fiber PMD emulator using an integrated series of thin-film micro-heaters," presented at the Optical Fiber Communication Conf. and Exhibit, Anaheim, CA, 2002, Paper ThA3.

[5] R. Khosravani, I. T. Lima, Jr., P. Ebrahimi, E. Ibragimov, A. E. Willner, and C. R. Menyuk, "Time and frequency domain characteristics of polarization-mode dispersion emulators," *IEEE Photon. Technol. Lett.*, vol. 13, no. 2, pp. 127–129, Feb. 2001.

[6] Y. K. Lize, L. Palmer, N. Godbout, S. Lacroix, and R. Kashyap, "Scalable polarization-mode dispersion emulator with proper first- and second-order statistics," *IEEE Photon. Technol. Lett.*, vol. 17, no. 11, pp. 2451–2453, Nov. 2005.

[7] M. Shtaif, "The Brownian-bridge method for simulating polarization mode dispersion in optical communications systems," *IEEE Photon. Technol. Lett.*, vol. 15, no. 1, pp. 51–53, Jan. 2003.

[8] M. Karlsson and J. Brentel, "Autocorrelation function of the polarization-mode dispersion vector," *Opt. Lett.*, vol. 24, no. 14, pp. 939–941, Jul. 1999.

[9] Q. Lin and G. Agrawal, "Correlation theory of polarization mode dispersion in optical fibers," *J. Opt. Soc. Amer. B, Opt. Phys.*, vol. 20, no. 2, pp. 292–301, Feb. 2003.

[10] M. Shtaif and A. Mecozzi, "Study of the frequency autocorrelation of the differential group delay in fibers with polarization mode dispersion," *Opt. Lett.*, vol. 25, no. 10, pp. 707–709, May 2000.

[11] B. S. Marks, I. T. J. Lima, and C. R. Menyuk, "Autocorrelation function for polarization mode dispersion emulators with rotators," *Opt. Lett.*, vol. 27, no. 13, pp. 1150–1152, Jul. 2002.

[12] L. Palmer, S. D. Dods, and P. M. Farrell, "Broad-band concatenated section PMD emulator design for low-interchannel correlation," *IEEE Photon. Technol. Lett.*, vol. 17, no. 5, pp. 1019–1021, May 2005.

[13] P. B. Phua and E. B. Ippen, "Combinatorial polarization scramblers for many-segment pmd emulator," *IEEE Photon. Technol. Lett.*, vol. 17, no. 2, pp. 405–407, Feb. 2005.

[14] L. Yan, Q. Yu, and A. E. Willner, "Uniformly distributed states of polarization on the Poincaré sphere using an improved polarization scrambling scheme," *Opt. Commun.*, vol. 249, no. 1–3, pp. 43–50, May 2005.

[15] T. Lu, D. O. Yevick, B. Hamilton, D. Dumas, and M. Reimer, "An experimental realization of biased multicanonical sampling," *IEEE Photon. Technol. Lett.*, vol. 17, no. 12, pp. 2583–2585, Dec. 2005.

[16] G. J. Foschini and C. D. Poole, "Statistical theory of polarization dispersion in single mode fibers," *J. Lightw. Technol.*, vol. 9, no. 11, pp. 1439–1456, Nov. 1991.

[17] J. P. Gordon and H. Kogelnik, "PMD fundamentals: Polarization mode dispersion in optical fibers," *Proc. Nat. Acad. Sci.*, vol. 97, no. 9, pp. 4541–4550, Apr. 2000.

[18] G. B. Arfken and H. J. Weber, *Mathematical Methods for Physicists*, 5th ed. San Diego, CA: Harcourt/Academic, 2001.

[19] M. Karlsson, J. Brentel, and P. A. Andrekson, "Long-term measurement of PMD and polarization drift in installed fibers," *J. Lightw. Technol.*, vol. 18, no. 7, pp. 941–951, Jul. 2000.

[20] A. Leon-Garcia, *Probability and Random Processes for Electrical Engineering*, 2nd ed. Reading, MA: Addison-Wesley, 1994.

[21] J. P. Marques de Sá, *Applied Statistics Using SPSS, STATISTICA and MATLAB*. New York: Springer-Verlag, 2003.

[22] B. L. Heffner, "Automated measurement of polarization mode dispersion using Jones matrix eigenanalysis," *IEEE Photon. Technol. Lett.*, vol. 4, no. 9, pp. 1066–1069, Sep. 1992.

[23] G. A. F. Seber and C. J. Wild, *Nonlinear Regression*. Hoboken, NJ: Wiley, 1989.

[24] L. Yan, M. C. Hauer, Y. Shi, X. S. Yao, P. Ebrahimi, Y. Wang, A. E. Willner, and W. L. Kath, "Polarization-mode-dispersion emulator using variable differential-group-delay (DGD) elements and its use for experimental importance sampling," *J. Lightw. Technol.*, vol. 22, no. 4, pp. 1051–1058, Apr. 2004.

[25] J. H. Lee, M. S. Kim, and Y. C. Chung, "Statistical PMD emulator using variable dgd elements," *IEEE Photon. Technol. Lett.*, vol. 15, no. 1, pp. 54–56, Jan. 2003.

[26] M. Karlsson, "Probability density functions of the differential group delay in optical fiber communication systems," *J. Lightw. Technol.*, vol. 19, no. 3, pp. 324–331, Mar. 2001.

Leigh Palmer (S'02) received the B.Sc. degree in physics and the B.E. degree in electrical engineering (Honors) from the University of Melbourne, Parkville, Victoria, Australia, in 2000 and 2001, respectively, where he is currently working toward the Ph.D. degree with the Department of Electrical and Electronic Engineering, focusing on accurately modeling and understanding polarization-mode-dispersion effects in optical networks.

Mr. Palmer is a member of the IEEE Lasers and Electro-Optics Society (LEOS) and the Optical Society of America (OSA).

Peter M. Farrell received the Ph.D. degree in atomic physics and laser spectroscopy from Griffith University, Brisbane, Qld., Australia, in 1992.

His interest in optical fiber communications systems stems from his postdoctoral employment with Telstra Research Laboratories, Clayton, Vic., Australia, where he worked on erbium-doped fiber amplifiers. He was an Optical Group Leader with Altamar Networks and an Associate Professor with Victoria University, Melbourne, Vic. He is currently an Associate Professor with the Department of Electrical and Electronic Engineering, University of Melbourne, Parkville, Vic. His research interests include optical fiber sensors, spectroscopy of rare-earth-doped glasses and fibers, and atomic spectroscopy.

Sarah D. Dods (S'97–M'01–SM'06) received the B.Sc. degree in physics (Honors) and the Ph.D. degree in electrical and electronic engineering from the University of Melbourne, Parkville, Victoria, Australia, in 1990 and 2000, respectively. Her doctoral topic is on in-band crosstalk in optical add–drop multiplexers.

Between 1990 and 2000, she worked with the research and development arm of Comalco, one of Australia's largest aluminum companies, working on various aspects of aluminum refining and smelting processes. Since 2000, she has worked for both the Australian Photonics Cooperative Research Centre's Photonics Research Laboratory, University of Melbourne, and VPI systems. She is currently a Senior Researcher with the National Information and Communication Technology (ICT) Australia Victoria Research Laboratory. Her current research interests cover signal-degradation mechanisms in optical transmission systems, optical performance monitoring, and 40-Gb/s system design.

Jamie S. Evans (S'93–M'98) was born in Newcastle, N.S.W., Australia, in 1970. He received the B.S. degree in physics and the B.E. degree in computer engineering from the University of Newcastle, Callaghan, N.S.W., in 1992 and 1993, respectively (awarded the University Medal upon graduation), and the M.S. and Ph.D. degrees in electrical engineering from the University of Melbourne, Parkville, Vic., Australia, in 1996 and 1998, respectively. He was awarded the Chancellors Prize for Excellence for his Ph.D. dissertation.

From March 1998 to June 1999, he was a Visiting Researcher with the Department of Electrical Engineering and Computer Science, University of California, Berkeley. He returned to Australia to take up a position as a Lecturer with the University of Sydney, Sydney, N.S.W., Australia, where he stayed until July 2001. Since then, he has been with the Department of Electrical and Electronic Engineering, University of Melbourne, where he is currently an Associate Professor. His research interests are in communications theory, information theory, and statistical signal processing with current focus on wireless communications networks.